Geophysical Research Letters

RESEARCH LETTER
10.1029/2023GL103230

The Effect of Indian Ocean Temperature on the Pacific Trade Winds and ENSO

Brady S. Ferster[1,2], Alexey V. Fedorov[2,3], Eric Guilyardi[2,4], and Juliette Mignot[2]

[1]Now at Department of Earth and Planetary Sciences, Yale University, New Haven, CT, USA, [2]LOCEAN-IPSL, Sorbonne Université, CNRS, IRD, MNHN, Paris, France, [3]Department of Earth and Planetary Sciences, Yale University, New Haven, CT, USA, [4]NCAS-Climate, University of Reading, Reading, UK

Key Points:

- Initial response to Indian Ocean warming (cooling) produces La Niña-like (El Niño-line) conditions in the tropical Pacific
- Equilibrium response to Indian Ocean warming (cooling) shows stronger (weaker) Pacific trade winds but warmer (colder) ocean temperatures
- Both warming and cooling of the Indian Ocean result in a stronger El Niño-Southern Oscillation due to greater positive feedbacks in the Bjerknes stability index

Supporting Information:

Supporting Information may be found in the online version of this article.

Correspondence to:

B. S. Ferster,
brady.ferster@locean.ipsl.fr

Citation:

Ferster, B. S., Fedorov, A. V., Guilyardi, E., & Mignot, J. (2023). The effect of Indian Ocean temperature on the Pacific trade winds and ENSO. *Geophysical Research Letters*, *50*, e2023GL103230. https://doi.org/10.1029/2023GL103230

Received 10 FEB 2023
Accepted 4 OCT 2023

Abstract A notable shift in the El Niño-Southern Oscillation (ENSO) has been observed in the early 21st century, characterized by an increased prevalence of Central Pacific (CP) events and strengthened Pacific trade winds. This shift may be attributed to the warming tropical Indian Ocean (TIO). To investigate this, we conduct perturbation experiments using the Insitut Pierre Simon Laplace climate model and nudge TIO surface temperatures to induce warming or cooling effects. Our findings reveal that TIO warming (or cooling) leads to amplified (weakened) mean trade winds and surface warming (cooling) in the Pacific region. Surprisingly, ENSO variability increases in both TIO cooling and warming scenarios. This result is linked to stronger positive feedbacks and a less stable Bjerknes index for either TIO forcing. Additionally, we find that TIO warming leads to more frequent CP events, meridional widening of wind anomalies, and broadening of the ENSO power spectrum toward lower frequencies.

Plain Language Summary The dominant mode of interannual climate variability, the El Niño-Southern Oscillation (ENSO), has visibly changed in the past three decades, with maximum sea surface temperature (SST) anomalies during El Niño events occurring in the Central Pacific (CP) rather than in the Eastern Pacific and having weaker magnitudes. Recent studies suggest that the observed stronger Pacific trade winds could have contributed to this shift. One possible mechanism driving such changes is the enhanced warming trends in the tropical Indian Ocean (TIO) relative to the rest of the tropics. Here, we conduct sensitivity experiments to investigate the effect of TIO SST on the Pacific. Our experiments with a climate model indicate that the Pacific trade winds change proportionally to the imposed forcing, with stronger trades corresponding to a warmer TIO. We find that ENSO variability increases strongly in the TIO cooling experiments, driven by weaker trade winds associated with TIO cooling. In the TIO warming experiments we find a shift toward CP-like events; however, we also observe a modest ENSO strengthening, which can be attributed to stronger positive feedbacks resulting from the remotely induced warming of the Pacific.

1. Introduction

The El Niño-Southern Oscillation (ENSO) is the main source of interannual climate variability, consisting of alternating warm (El Niño) and cold (La Niña) phases with irregular 2–7 years cycles (e.g., McPhaden et al., 2020). ENSO is driven by ocean-atmosphere interactions in the tropical Pacific, involving positive Bjerknes feedback (Bjerknes, 1969) and negative feedbacks associated with ocean memory and damping processes (Jin, 1997).

ENSO's decadal modulation causes variations in the strength of El Niño events, such that weaker El Niño events (2000s and 2010s) can follow decades with a strong El Niño (1980s and 1990s) (Fedorov et al., 2020). This modulation also affects the type of El Niño, corresponding to the location of the maximum sea surface temperature (SST) anomalies. For example, Central Pacific (CP) El Niño events characterized by anomalies in the central tropical Pacific (west of 150°W) have been dominant in the early 21st century, while Eastern Pacific (EP) events dominated the record in the two preceding decades (e.g., Capotondi et al., 2015).

Since ENSO critically depends on the Pacific mean state (Cai et al., 2015; Fedorov & Philander, 2000, 2001; Fedorov et al., 2020), externally driven changes have been proposed as one of the potential causes of ENSO decadal modulation. Such mean state changes in the Pacific can be induced from other tropical basins, including the Indian Ocean (Mayer & Balmaseda, 2021). Accordingly, the focus of the present study is the effect of mean SST changes in the Indian Ocean on the Pacific mean state and ENSO. Since 1950s, the tropical Indian Ocean (TIO) has been steadily warming by 0.15°C per decade and warming 0.05°C per decade faster than the

remaining tropical basins (Atlantic and Pacific) (Hu & Fedorov, 2019). These relative TIO temperature anomalies, compared to the remaining tropical ocean, are hereafter referred as rTIO. This rTIO warming can have strong global impacts through atmospheric and oceanic teleconnections (Fletcher & Cassou, 2015; Hardiman et al., 2020). Furthermore, a sudden TIO warming can arrest El Niño development (Dong & McPhaden, 2018). However, our approach is different from their study and focuses on a quasi-equilibrium response of the tropical Pacific and ENSO to TIO temperature changes.

ENSO is understood to originate from instability of the tropical Pacific mean state caused by ocean-atmosphere interactions, and broad literature exists on the effects of mean state on ENSO (reviewed in Fedorov et al. (2020)). One conclusion, ranging from experiments using intermediate-complexity (Zebiak & Cane, 1987) and similar models (An & Jin, 2000; An & Wang, 2000; Fedorov & Philander, 2000, 2001) to idealized studies with coupled GCMs (Fedorov et al., 2020; Hu & Fedorov, 2018, 2019; Zhao & Fedorov, 2020) is that the weakening (strengthening) of mean Pacific trade winds typically tends to intensify (weaken) ENSO. Several studies have highlighted the resulting variability, feedbacks, and structure of ENSO in the CMIP5 and CMIP6 models compared to observations (Beobide-Arsuaga et al., 2021; Cai et al., 2018; Ferrett & Collins, 2019; Heede & Fedorov, 2023b; Jiang et al., 2021; Lu et al., 2018). In those studies, there is no clear consensus on how changes in the background state of the tropics can shape ENSO variability and characteristics on decadal and longer timescales (Beobide-Arsuaga et al., 2021; Cai et al., 2015; Collins et al., 2010; Fredriksen et al., 2020; Guilyardi et al., 2009, 2012; Stevenson et al., 2021; Yeh et al., 2018). Nevertheless, a broad range of global warming experiments within CMIP6 suggests a strengthening of future ENSO, which in part might be explained by the future weakening of the Pacific trade winds and the Walker circulation (Heede & Fedorov, 2021, 2023b).

Separating internal variability and the anthropogenic signal has proved challenging, as interannual variability can influence low-frequency patterns and the mean state (Fedorov et al., 2020). In CMIP5 historical simulations, 90% of the response of ENSO amplitude and SST changes can be explained by internal variability (Maher et al., 2018). Typical 100-year simulations, such as the historical or warming scenarios would require 50 ensemble members to achieve an accuracy of ENSO variability within 5% of the truth (Lee et al., 2021; Milinski et al., 2020), highlighting the difficulty of understanding transient changes in climate.

Given these challenges, it is important to continue researching the response of ENSO to mean state changes. In our study, we conducted sensitivity experiments by increasing or decreasing TIO surface temperature to examine the impact on the tropical Pacific mean climate and ENSO variability. We found that warming the TIO region strengthens the Pacific Walker circulation and trade winds due to increased convection, while cooling the TIO has the opposite effect. However, the warming of the Indian Ocean also efficiently warms the Pacific, which complicates the ENSO response. Overall, our study highlights the complex interactions between the Indian Ocean and the Pacific mean state, shedding light on the factors influencing ENSO variability.

2. Model and Experimental Configuration

2.1. Model Configuration and Experimental Setup

We use the coupled climate model IPSLCM6A-LR (IPSL-CM6 thereafter), developed at the Institut Pierre-Simon Laplace and participating in CMIP6. The model configuration is described by Boucher et al. (2020) and Mignot et al. (2021); its evaluation in terms of ENSO metrics can be found in Planton et al. (2021). Specifically, IPSL-CM6 has a good representation of the ENSO amplitude and asymmetry, however, underperforms in ENSO seasonality (Figure 2 of Planton et al. (2021)). The experimental design of the perturbation experiments and the atmospheric and oceanic responses to nudging the TIO are detailed in Ferster et al. (2021) and summarized below.

To increase or decrease mean rTIO, a simple Newtonian relaxation (or nudging) of TIO surface temperature is imposed at each timestep, using the same model-year of the 1,100 years-long IPSL-CM6 piControl (referred as piControl) as the starting point. The TIO region is defined as 30°–100°E, 30°S–30°N and is continuously nudged toward monthly SST values of the corresponding piControl segment to which anomalies of −2°C, −1°C, +1°C, and +2°C are respectively added. This experimental design allows us to maintain the natural variability of the tropics while nudging the tropical Indian basin. These perturbation experiments are referred to as TIOxC, where "x" denotes to the value of TIO target temperature.

A fixed surface restoring value of -40 W m^{-2} K^{-1} is applied, resulting in approximate mean SST changes in the TIO of −1.4°C, −0.7°C, +0.7°C, and +1.4°C from the control respectively. As expected, the final changes in SST

are smaller than the nudging target temperatures (see Figure S1 in Supporting Information S1). The corresponding rTIO changes are even smaller (−0.7°C, −0.3°C, +0.3°C, and +0.6°C) since the warming (cooling) of TIO increases (decreases) SST remotely in the Pacific Ocean as well.

To assess the effect of the nudging procedure on the climate system, we also conduct an experiment with the target temperature of 0°C. The inclusion of the TIO = 0°C experiment can be thought of adding white noise at each timestep, as the nudging is relatively weak, and the experiment maintains independent variability. We find little difference between the TIO = 0°C experiment and the piControl (further see Section 3.2). The perturbation experiments are extended to 950-year to allow for a robust statistical analysis of the achieved quasi-equilibrium state. The TIO − 2°C analysis is stopped at year 500 following the near-collapse of Atlantic Meridional Overturning Circulation (AMOC) (Ferster et al., 2021).

Hu and Fedorov (2019) report that the TIO (rTIO) have been steadily warming since the 1950s by 0.15°C (0.05°C) per decade which is approximately equivalent to +1°C warming in the TIO and a 0.3°C rTIO anomaly that developed over the past 70 years. Therefore, the magnitude of the imposed +1°C nudging experiment compares well with these observations. The other experiments serve to investigate the overall sensitivity of the tropical Pacific basin to TIO changes, and the results are discussed mostly in the context of the TIO + 1°C experiment.

2.2. Computing the Bjerknes Stability Index and Power Spectra

The Niño3 region is defined as 5°S to 5°N and 150° to 90°W, and the Niño 3.4 and Niño 4 regions as 170° to 120°W and 160°E to 150°W, respectively. A simple approach can be used to define CP El Niño through the Niño 4 index and the EP El Niño through the Niño 3 index, while the Niño 3.4 index defines a combination of the two El Niño flavors (e.g., Fedorov et al., 2015).

To assess the system's stability, we use the Bjerknes stability index (BJ index for short) which describes the collective strength of feedbacks and damping terms that affect the stability of ENSO under the recharge oscillator approximation (i.e., Jin, 1997; Jin et al., 2006, 2020). Here, we follow the computation of the BJ index by Ferrett and Collins (2019):

$$I_{BJ} = \frac{R}{2} - \varepsilon; \quad R = \mathrm{ZA} + \mathrm{EK} + \mathrm{TC} + \mathrm{CD} + \mathrm{TD} \tag{1}$$

$$R = \mu_a\beta_u\left\langle\frac{-\partial T}{\partial x}\right\rangle_E + \mu_a\beta_w\left\langle\frac{-\partial T}{\partial z}\right\rangle_E + \mu_a\beta_h\left\langle\frac{w}{H_1}\right\rangle_E - \left(\frac{\langle u\rangle_E}{L_x} + \frac{\langle -2yv\rangle_E}{L_y^2} + \frac{\langle H(w)W\rangle_E}{H}\right) - \alpha_s \tag{2}$$

R describes net positive and negative feedbacks affecting SST evolution and the constant ε accounts for the mechanical damping of thermocline anomalies. The BJ index (I_{BJ}) gives the growth or decay rate of the ENSO mode, which has similarly been used in previous literature (Ferrett & Collins, 2019; Jin et al., 2020; Manucharyan & Fedorov, 2014; Zhao & Fedorov, 2020). Here, the BJ index is broken down into five main components in Equations 1 and 2, including the zonal advection, Ekman (EK), and thermocline (TC) feedbacks, and the net current damping and thermodynamic damping (TD) feedbacks. Respectively, these represent the positive feedbacks and damping feedbacks of the BJ index.

The calculation involves area-averaging over the east equatorial Pacific region (180°E–80°W, 5°S–5°N). The surface currents (u, v) and upwelling current (w) are considered as a time mean. Upwelling is determined by a step function assigning 0 for negative values ($H(w) = 0$ for $w < 0$) and 1 for positive values ($H(w) = 1$ for $w > 0$). The averaging region's longitudinal (L_x) and latitudinal (L_y) extents are considered, assuming a mixed layer depth (H_m) of 50 m. The TD term (α) is determined by regressing heat flux anomalies onto SST anomalies. Bjerknes feedback components are estimated through regressions: μ_a (mu) for wind stress anomalies against SST anomalies, β_u (beta$_u$) for zonal surface ocean current anomalies against surface wind stress anomalies, β_w (beta$_w$) for upwelling ocean current against surface wind stress anomalies, and β_h (beta$_h$) for thermocline slope anomalies against surface wind stress anomalies. Finally, the feedback components are combined to obtain the total Bjerknes Index, with heat flux damping normalized using the heat capacity of water ($c_p = 4180$ J kg^{-1} K^{-1}), and the density of seawater ($\rho = 1{,}029$ kg m^{-3}). This comprehensive analysis allows for an understanding of the interactions between ocean currents, wind stress, and heat exchange in the equatorial Pacific region.

The power spectra analysis of the following Niño timeseries uses a variance preserving approach: the power spectral density is multiplied by the frequency and the frequency is shown as logarithmic. The analysis furthermore

applies a multi-taper approach (Park et al., 1987; Thomson, 1982; Yu & Fedorov, 2022). In the analyses, the initial 200 years of the warming and cooling experiments are excluded to allow the climate to adjust to the nudging, which includes changes to the AMOC (Ferster et al., 2021) and the results indicate at least 150 years of an experiment are required to produce nearly identical power spectra and ENSO variability results.

Figure S1 in Supporting Information S1 displays the adjustment of the rTIO and Niño 3.4 SST (Figures S1a and S1b in Supporting Information S1) on decadal timescales, but the Indonesian Throughflow (ITF) and AMOC (Figures S1c and S1d in Supporting Information S1) reach a quasi-equilibrium after roughly two centuries in the experiments, albeit a longer adjustment time in the case of the TIO − 2°C experiment. Monthly anomalies are computed by removing the monthly climatology of each respective experiment. Since Niño 3 and Niño 3.4 analyses produced similar results, we will focus on Niño 3.4 in the manuscript.

3. Results

3.1. Changes in the Mean State: Pacific Trade Winds, SST, and Upper Ocean Temperature

The initial response to the warming or cooling of the TIO leads to a rapid development of quasi-stationary equatorial Rossby and Kelvin waves originating from the TIO, as well as extra-tropical Rossby waves propagating poleward in both hemispheres (Figures S2a–S2c in Supporting Information S1). The anomalous response of geopotential height drives anomalous zonal and meridional wind stress across the equatorial Pacific and globally (Figures S2d–S2i in Supporting Information S1). The Rossby wave response originating from the TIO generates approximately the same spatial patterns, albeit of opposite signs and different magnitudes between the warming and cooling experiments. Warming the TIO drives the intensification of trade winds on monthly timescales, leading to La Niña-like conditions with negative SST anomalies and increased thermocline slope within the equatorial Pacific within the start of the experiment (Figures S3a and S3b in Supporting Information S1, averaged over the first 5 years of the experiment). The opposite pattern is seen in the cooling experiments, driving El Niño-like conditions and decreased easterlies in the tropical Pacific (Figures S3c and S3d in Supporting Information S1). These results are similar to Zhang and Karnauskas' (2017) and Mayer and Balmaseda (2021), finding that warming the TIO creates a zonal tropical gradient, intensifying the Walker circulation. This enhanced circulation has been shown to result in the observed strengthening of the tropical Pacific easterlies and to a La Niña-like state (Luo et al., 2012), and within a year can cause weaker ITF transports and a shoaling thermocline in the western Pacific. This may also corroborate the results of Dong and McPhaden (2018) that an anomalous warming of the Indian Ocean can suppress a developing El Niño event in the Pacific.

After the initial response, a more gradual transition to a quasi-equilibrium state in the upper Pacific Ocean takes place, which requires over half-a-century for higher frequency variability, such as ENSO, and several centuries for low frequency signals, such as the ITF and AMOC (Figure S1 in Supporting Information S1). In this quasi-equilibrium state, TIO warming results in enhanced equatorial easterlies in the Pacific, a deepening of the equatorial thermocline in the west, and SST warming throughout the tropical and subtropical Pacific (Figures 1a and 1b; Figures S2f and S4 in Supporting Information S1). In the western Indian Ocean, a significant warming develops within the surface 100 m due to anomalous westerly winds generated along the equator as part of the Matsuno-Gill response to warming (Gill, 1980; Hu & Fedorov, 2019; Matsuno, 1966) and the corresponding deepening of the thermocline. At the same time, a cooling develops in the subsurface eastern Indian Ocean (below 200 m), contributing to upwelling and reduced SST anomalies in the western TIO compared to the eastern TIO basin. The response is roughly opposite in the TIO cooling experiments, with a significant strengthening of the trade winds in the Pacific but anomalous easterly winds in the Indian Ocean (Figures 1c and 1d; Figure S2d in Supporting Information S1).

The main difference between the cooling and warming experiments in terms of mean state changes in the Pacific is that TIO warming induces a smaller quasi-equilibrium change in zonal wind stress magnitude along the equator (Figure 2a, Figure S4a in Supporting Information S1) than the TIO cooling does. This asymmetry arises largely because the absolute magnitude of the induced warming of the Pacific is greater than the magnitude of Pacific cooling (Figure 2b), so that in the former case only a very modest strengthening of the interbasin Indo-Pacific SST contrast takes place. This is consistent with the results implied by the study of Zhang and Karnauskas (2017) on the role of interbasin temperature gradients for the Walker circulation.

Furthermore, the warming experiments result in a uniform deepening of the thermocline across the equatorial Pacific and increased sea surface height (SSH) (Figure 1 and Figure S4 in Supporting Information S1), while in the cooling experiments there is a significant reduction of the east-west SSH contrast along the equator. The compensating effects

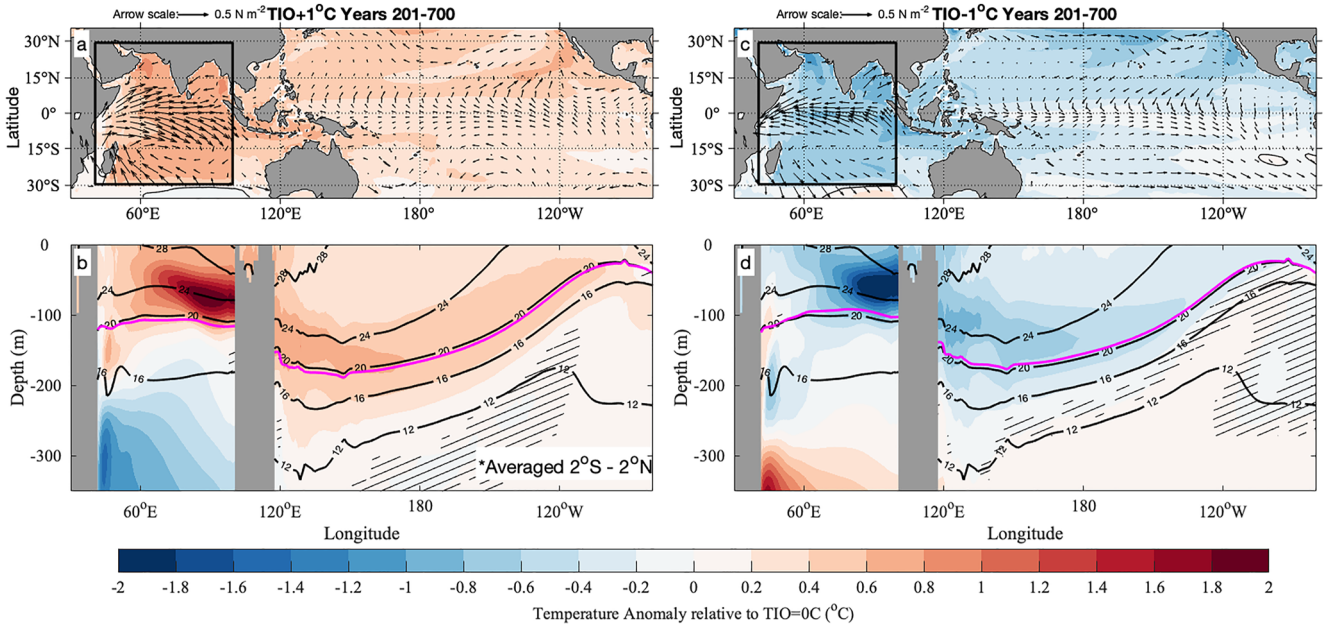

Figure 1. Mean temperature anomalies in °C for the (a, b) TIO+1°C and (c, d) TIO−1°C experiments for years 200–700 relative to the tropical Indian Ocean (TIO) = 0°C (experiment control) time mean, representing the quasi-equilibrium difference. Top panels show anomalous sea surface temperature (SST) and surface wind stress (arrows); the thin black contour separates cold and warm anomalies. The black box indicates the TIO region used for SST nudging. Bottom panels show mean anomalies in potential temperature averaged between 2°S and 2°N for the same longitudes. Black isotherms represent mean ocean temperature in the control while the magenta line indicates the 20°C isotherm from the respective sensitivity experiments. Hashing in the bottom plots represent anomalies that are not significantly different to the 95% confidence interval of TIO = 0°C experiment using a two-sided t-t-test.

explain why in the warming experiments, this SSH contrast barely changes, reflecting the reduced net effect of the wind stress changes compared to temperature changes on the mean state (Figure S4 in Supporting Information S1). In the cooling experiments, the reduction of the SSH contrast is directly related to the weakening of the trade winds.

3.2. ENSO Changes

The next question to explore is how these mean state changes affect ENSO. Surprisingly, we find that both sets of experiments result in the increased ENSO amplitude described for example, by the Standard Deviation (Std.Dev.) of interannual SST anomalies, see Figures 2c and 3, Figure S5 in Supporting Information S1. The strengthening of ENSO SST amplitude is greater in the TIO cooling experiments, with a significant increase throughout the equatorial Pacific compared to both the piControl and TIO = 0°C experiments. In the warming experiments, Std.Dev. significantly increases in the central and western equatorial Pacific, implying a more frequent occurrence of CP El Niño events, which is expected for stronger trade winds (Zhao & Fedorov, 2020). Spatial changes of SST Std.Dev. (Figure 3, Figure S5 in Supporting Information S1) confirm these findings: the TIO cooling experiments result in a narrow band of increased SST variability by 0.1–0.2°C in the central and eastern equatorial Pacific, while warming the TIO produces a pattern of increased SST variability (0.05–0.15°C) in the western and central equatorial Pacific.

In addition, comparing the experiment TIO = 0°C and piControl, we find no significant differences in the simulated mean state and ENSO (Figure 2c, Figure S5 in Supporting Information S1). In fact, the mean states in the two experiments are nearly indistinguishable (Figures S4 and S5 in Supporting Information S1). This suggests that the method employed minimizes the impact of reducing the TIO variability on the Pacific mean state and ENSO variability, as was the motivation to apply such method in our nudging protocol.

3.3. Mechanisms of ENSO Changes

To explain ENSO changes in the perturbation experiments, we compute the BJ index and its components for the Niño 3.4 region (Figures 4a–4c, Figures S6 and S7 in Supporting Information S1). We find that for all experiments the Bjerknes index has negative values, indicating a weakly damped system. For both warming and cooling experiments the BJ index becomes less negative, suggesting a lower ENSO stability compared to the piControl and TIO = 0°C simulations. Comparatively, the cooling experiments show lower stability than the warming

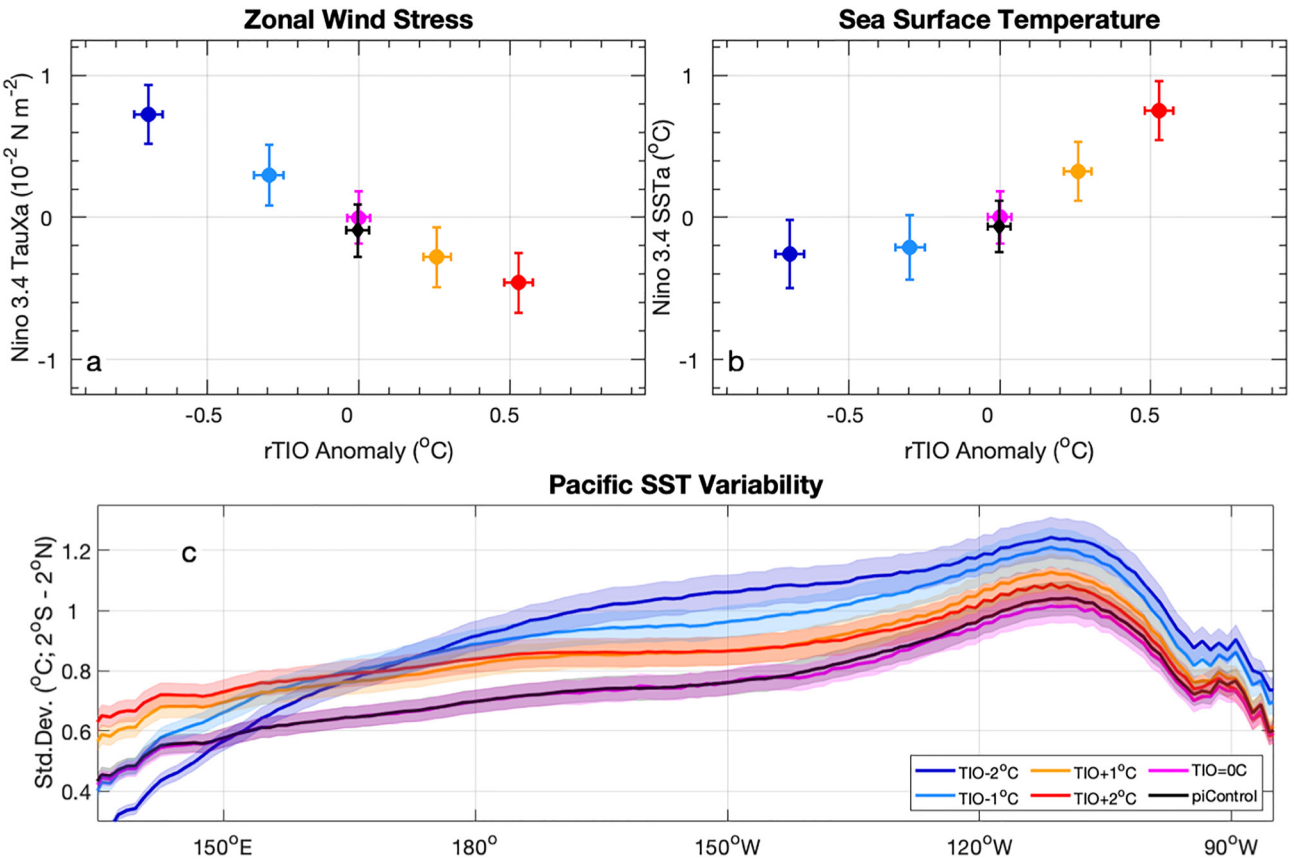

Figure 2. (a) Zonal wind stress and (b) sea surface temperature (SST) anomalies in the Niño 3.4 region relative to the tropical Indian Ocean (TIO) = 0°C (experiment control). The *x*-axis represents the mean rTIO anomaly in the respective experiments, hence, the TIO = 0°C is plotted at 0. Negative values in panel (a) denote the strengthening of easterly winds. (c) SST standard deviation along the equator in the Pacific based on interannual SST anomalies averaged between 2°S and 2°N. Error bars and shading for the experiments represent the 95% confidence interval of the upper and lower bounds.

experiments. Thus, in both sets of experiments, changes in the BJ index toward lower stability are consistent with the simulated strengthening of ENSO (Figure 2c).

The changes in the Bjerknes index (Figure 4a) in these experiments can largely be explained by stronger net positive feedbacks (Figure 4b), which includes the thermocline (TC), advection, and Ekman (EK) feedbacks (Figures S6a–S6c in Supporting Information S1). At the same time, the competing damping by the mean currents (Figures S6d and S6e in Supporting Information S1) results in slightly weaker net damping effects compared to the control (Figure 4c). Therefore, the increase in ENSO variability in both warming and cooling experiments is largely driven by the effects of positive feedbacks (especially, of the TC and EK feedbacks).

We further investigate the critical components that drive changes in the TC and EK feedbacks. First, focusing on the TIO − 2°C experiment, we find that the coupling coefficient μ between the zonal wind stress and Niño 3.4 SST decreases relative to the control. However, in this experiment, the thermocline (β_h) and upwelling (β_w) coupling to wind stress increase by about 30%, which largely explains the lower stability of the system (i.e., a less negative BJ index). In the warming experiments, increases in μ and β_h components relative to the control appear to be critical in strengthening the TC feedback and thus making the system less stable.

As discussed earlier, equatorial easterlies in the Pacific consistently decrease in the cooling experiments. Previous work suggests that the weakening of Pacific trade winds should result in ENSO intensification (Fedorov & Philander, 2000, 2001; Zhao & Fedorov, 2020; among others), which is consistent with our results, and the stronger ENSO can be explained by the strengthening of the thermocline, advection, and/or Ekman feedbacks. On the other hand, the strengthening of Pacific trades in the warming experiments should, in general, suppress El Niño, but instead we observe a modest ENSO strengthening. Part of the disagreement can be explained by the minimal increase in zonal winds, resulting in barely any changes in the east-west SSH gradient along the equator

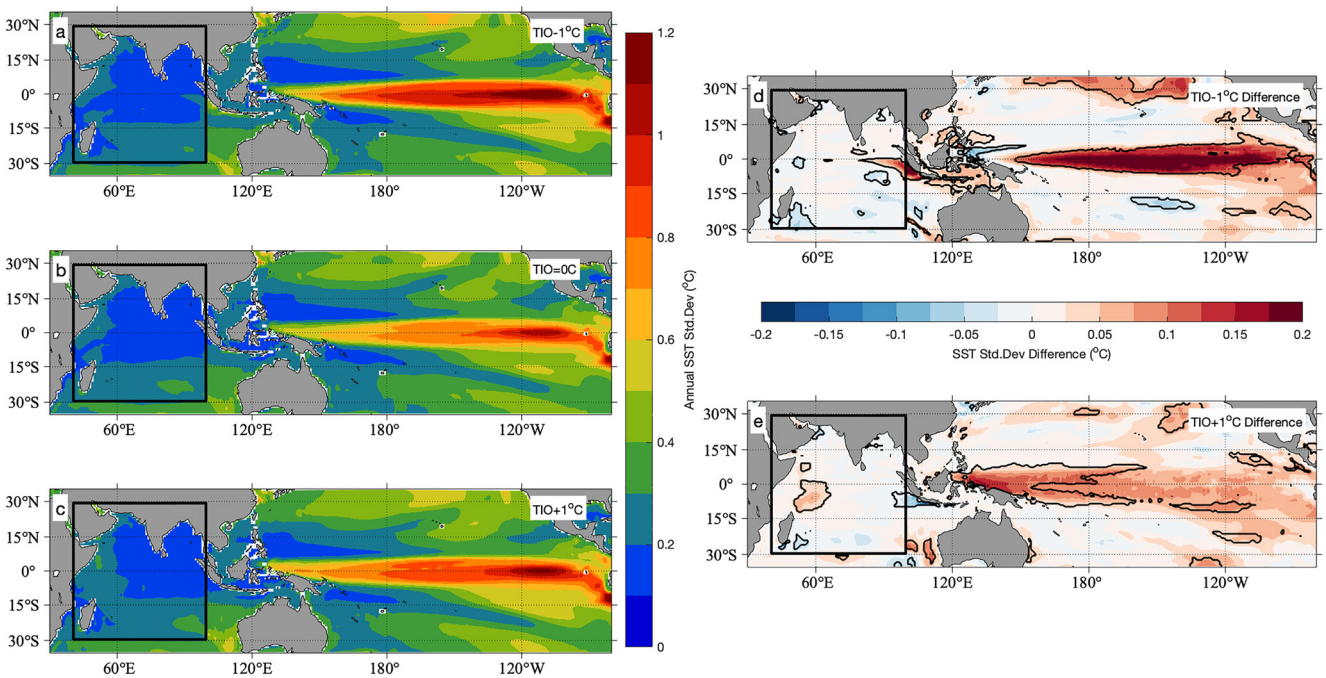

Figure 3. Interannual sea surface temperature (SST) variability (standard deviation) in the (a) TIO−1°C, (b) tropical Indian Ocean (TIO) = 0°C (experiment control), and (c) TIO+1°C experiments, and the (d, e) differences of the sensitivity experiments relative to the control. Thin contours mark the regions where variability exceeds the 95% confidence interval of the TIO = 0°C using an *F*-test. The black box represents the TIO region used for SST nudging. Hereafter, the results for perturbation experiments are computed starting from year 101 until the end of each simulation (unless stated differently).

(Figure S4b in Supporting Information S1). In contrast, these small changes are accompanied by a significant warming of the Pacific Ocean which can act to increase ocean-atmosphere coupling as discussed above.

Other factors that may contribute to the stronger ENSO in the warming experiments include changes in the meridional structure of ENSO wind anomalies, which is not considered by the BJ index. Specifically, we regress monthly zonal wind stress anomalies in the Pacific onto the Niño 3.4 SST index (Figures 4d and 4e), following Capotondi et al. (2006). This regression shows the typical structure of zonal wind stress anomalies associated with ENSO. In this analysis, we find a robust meridional expansion of these anomalies with TIO warming in mainly the Southern Hemisphere (Figure 4d; by nearly 4° of latitude in the TIO + 2°C experiment), while a contraction in the cooling experiments that occurs mostly in the Northern Hemisphere. In a simple ENSO model (Fedorov, 2010), a meridional expansion of wind stress anomalies shifts ENSO toward longer periods and simultaneously makes the system more unstable, leading to a stronger ENSO. This is consistent with a number of coupled model studies (Capotondi et al., 2006; Deser et al., 2006).

Finally, in observations, ENSO occurs irregularly with 2–6 years cycles. Analyzing power spectra for the experiments, we find that the piControl and TIO = 0°C simulations peak at 3–4 years in both Niño 3.4 and Niño 4 time series (Figures 4f and 4g). For both time series, the cooling experiments result in a significant increase in the power spectral density in the 3–4 years band. The warming experiments, however, show no increase in the 3–4 years band (and a slight decrease for the TIO + 2°C experiment). Instead, there is an increase in the power spectral density at lower frequencies, in the 6–9 years band. Thus, the warming experiments show a broadening of the power spectrum with a shift toward lower frequency variability in the region compared to the control. This broadening of the power spectrum and the increase in the power spectral density at lower frequencies also becomes evident when the simulated ENSO variability is divided into two frequency bands—corresponding to periods longer (6–10 years) and shorter (2–6 years) than 6 years (Figures S8a and S8b in Supporting Information S1).

4. Conclusions

In our experiments, we studied the impact of Indian Ocean temperature changes on the tropical Pacific mean state and ENSO variability. Initially (years 1–5), TIO warming (cooling) strengthened (weakened) Pacific trade

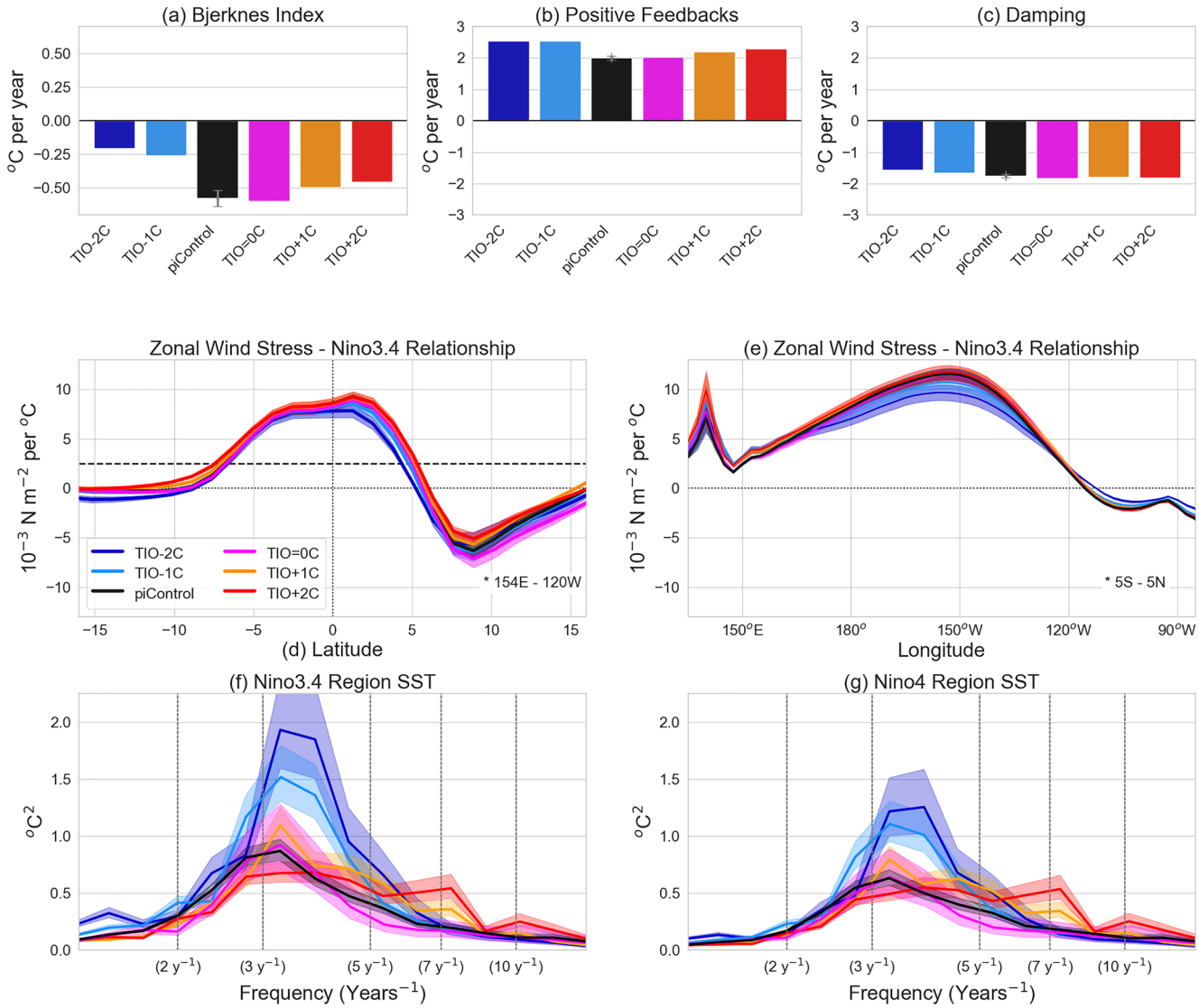

Figure 4. (a) The Bjerknes stability index estimated for the Niño 3.4 region in °C per year, (b) the positive feedbacks, and (c) damping effects of the index. (d) The meridional and (e) zonal structure of monthly zonal wind stress anomalies regressed upon the Niño 3.4 index. (d) Is zonally averaged between 154°E to 120°W (similar to Figure 7 in Capotondi et al. (2006)) and (e) is meridionally averaged between 5°S and 5°N. The values on the top left in (d) represent the width of positive wind stress anomalies around the equator and quantify the broadening of these anomalies in warm experiments relative to cold experiments. (f, g) Power spectra for the Niño 3.4 and 4 indices (°C^2) from monthly anomalies using a "variance preserving" approach, in which the power spectral density is multiplied by the frequency and the frequency is shown as logarithmic. Niño 3 is not shown, as it is similar to the Niño 3.4 results. Note that the increase in El Niño-Southern Oscillation variability in tropical Indian Ocean (TIO) warming experiments is associated with an expansion toward lower frequencies as compared to the TIO = 0°C (experiment control). Error bars in panels (a–c) represent the standard error with 95% confidence interval using the piControl simulation broken into four different chunks of 400 years. Shading in (d, e) is the 95% confidence interval of the zonal or meridional averaged values.

winds, leading to La Niña (El Niño)-like conditions due to the Bjerknes feedback. This initial response resembled previous findings that an increased tropical zonal temperature gradient can drive Pacific easterly wind strengthening and EP cooling (Heede & Fedorov, 2023a; Luo et al., 2012; Zhang & Karnauskas, 2017). Moreover, the initial response to TIO warming demonstrates similarities to the observed changes in the 2000s relative to the 1980–1990s with increased Pacific trade winds and colder eastern equatorial Pacific. Such changes could result in a weakening of the thermocline feedback and a dampened ENSO cycle (Lübbecke & McPhaden, 2014; Zhao & Fedorov, 2020). However, the long-term quasi-equilibrium state showed a more complex picture.

The quasi-equilibrium of the TIO cooling experiments show a strong weakening of the Pacific easterly winds, accompanied by a small decrease in the equatorial Pacific SST. Consequently, the trade wind weakening

dominates the mean state changes, leading to a stronger ENSO as suggested by previous studies and the system's lower stability inferred from the BJ index. Conversely, TIO warming significantly warmed the tropical Pacific, reducing the rTIO temperature and moderating trade wind strengthening. This more modest trade wind change, combined with the tropical Pacific warming, results in a slight strengthening of ENSO that is also predicted by the BJ index. It is accompanied by a broadening of the ENSO spectrum toward decadal frequencies, likely caused by the meridional widening of ENSO wind stress anomalies (Capotondi et al., 2006; Fedorov, 2010). In addition, the TIO warming experiments show increased SST variability largely in the central and western Pacific rather than the eastern equatorial Pacific, suggesting a higher likelihood of CP El Niño events under TIO warming. Overall, the quasi-equilibrium response differs from the initial transient response of the experiments and, arguably, to the observed changes of the past few decades, with apparently a more stable ENSO mode.

Our results demonstrate that in a quasi-equilibrium decreasing or increasing the mean SST gradient between the tropical Indian and Pacific basins reduces tropical Pacific stability, increasing ENSO variance. Other studies have examined the impact of changes in Pacific mean state and winds on ENSO (Fedorov et al., 2020; Ferrett & Collins, 2019; Heede & Fedorov, 2023b; Hu & Fedorov, 2018; Manucharyan & Fedorov, 2014; Siuts et al., 2022; Tan et al., 2020; Zhao & Fedorov, 2020). In several cases the results can be explained by changes in the BJ index, as in our study, but other factors like atmospheric noise or nonlinearity can also become important and need to be considered in addition to the BJ index. Nonlinearity and the impact of quasi-stationary Rossby waves on wind patterns are also important (Graham et al., 2014) and may contribute to non-uniform changes in Pacific trade winds.

Additional caveats to consider include the new Arctic sea ice state, long-term changes in AMOC and ITF, and changes in other types of tropical variability, such as the Madden-Julien Oscillation (Tan et al., 2020). For example, in the TIO – 2°C experiment, a weakened AMOC state could potentially promote increased ENSO variability though weaker cross-equatorial winds and stronger positive feedbacks in the eastern equatorial Pacific (Liu et al., 2023). However, these effects appear to be weaker than the direct impact of zonal wind weakening (Zhao & Fedorov, 2020). A notable difference in the tropical Pacific SST is the transient negative and the positive quasi-equilibrium anomalous response, which can partially be explained by the methods of nudging and the radiative effect across the tropics (see Ferster et al. (2021) and Hu and Fedorov (2019)). Finally, it remains to be seen how robust the small strengthening of ENSO with TIO warming is in other models.

Overall, our results highlight the significance of the inter-tropical zonal SST gradients and the TIO warming. Using the rate of warming from Hu and Fedorov (2019), the TIO + 1°C closely resembles observed warming trend, albeit in a quasi-equilibrium state. This has implications for future climate change and its modulation of the tropical Pacific response to global warming, suggesting that the enhanced warming of the TIO could contribute to the increased occurrence of CP El Niño events and delay the expected weakening of the Walker circulation (e.g., Heede & Fedorov, 2023a).

Acknowledgments
This research is supported by the ARCHANGE project of the "Make our planet great again" program (ANR-18-MPGA-0001, France). Additional support is provided to AVF by NOAA (NA20OAR4310377), NSF (AGS-2053096), and DOE (DE-SC0023134). JM is supported by the ANR-19-JPOC-003 JPI climate/JPI ocean ROADMAP project. This work used the HPC resources of TGCC under the allocations provided by Grand Equipement National de Calcul Intensif (GENCI) and benefited from the Ensemble de Services Pour la Recherche l'IPSL (ESPRI) computing and data centre (https://mesocentre.ipsl.fr) which is supported by CNRS, Sorbonne University, Ecole Polytechnique, and CNES and through national and international grants. The authors would like to thank Sam Ferrett and Mat Collins for their help with the BJ index code/script, and the three anonymous reviewers for their beneficial feedback.

Data Availability Statement

The data sets generated during the experiment are located on the TGCC machine Irene. Several data sets to reproduce the results of the manuscript are published as Ferster et al. (2023a, 2023b, 2023c) (cooling experiments, warming experiments, and control experiments, respectively) and details to access the public threads of all the model output for each of the experiments on the TGCC machine are found with the corresponding published data sets. The IPSL pre-industrial control data sets are publicly available on the CMIP6 ESGF servers (i.e., IPSL: https://esgf-node.ipsl.upmc.fr/search/cmip6-ipsl/).

References

An, S.-I., & Jin, F.-F. (2000). An Eigen analysis of the interdecadal changes in the structure and frequency of ENSO mode. *Geophysical Research Letters*, *27*(16), 2573–2576. https://doi.org/10.1029/1999GL011090

An, S.-I., & Wang, B. (2000). Interdecadal change of the structure of the ENSO mode and its impact on the ENSO frequency. *Journal of Climate*, *13*(12), 2044–2055. https://doi.org/10.1175/1520-0442(2000)013<2044:ICOTSO>2.0.CO;2

Beobide-Arsuaga, G., Bayr, T., Reintges, A., & Latif, M. (2021). Uncertainty of ENSO-amplitude projections in CMIP5 and CMIP6 models. *Climate Dynamics*, *56*(11–12), 3875–3888. https://doi.org/10.1007/s00382-021-05673-4

Bjerknes, J. (1969). Atmospheric teleconnections from the equatorial Pacific 1. *Monthly Weather Review*, *97*(3), 163–172. https://doi.org/10.1175/1520-0493(1969)097<0163:ATFTEP>2.3.CO;2

Boucher, O., Servonnat, J., Albright, A. L., Aumont, O., Balkanski, Y., Bastrikov, V., et al. (2020). Presentation and evaluation of the IPSL-CM6A-LR climate model. *Journal of Advances in Modeling Earth Systems*, *12*(7), e2019MS002010. https://doi.org/10.1029/2019MS002010

Cai, W., Santoso, A., Wang, G., Yeh, S.-W., An, S.-I., Cobb, K. M., et al. (2015). ENSO and greenhouse warming. *Nature Climate Change*, *5*(9), 849–859. https://doi.org/10.1038/nclimate2743

Cai, W., Wang, G., Dewitte, B., Wu, L., Santoso, A., Takahashi, K., et al. (2018). Increased variability of eastern Pacific El Niño under greenhouse warming. *Nature*, *564*(7735), 201–206. https://doi.org/10.1038/s41586-018-0776-9

Capotondi, A., Wittenberg, A., & Masina, S. (2006). Spatial and temporal structure of Tropical Pacific interannual variability in 20th century coupled simulations. *Ocean Modelling*, *15*(3–4), 274–298. https://doi.org/10.1016/j.ocemod.2006.02.004

Capotondi, A., Wittenberg, A. T., Newman, M., Di Lorenzo, E., Yu, J.-Y., Braconnot, P., et al. (2015). Understanding ENSO diversity. *Bulletin of the American Meteorological Society*, *96*(6), 921–938. https://doi.org/10.1175/BAMS-D-13-00117.1

Collins, M., An, S.-I., Cai, W., Ganachaud, A., Guilyardi, E., Jin, F.-F., et al. (2010). The impact of global warming on the tropical Pacific Ocean and El Niño. *Nature Geoscience*, *3*(6), 391–397. https://doi.org/10.1038/ngeo868

Deser, C., Capotondi, A., Saravanan, R., & Phillips, A. S. (2006). Tropical Pacific and Atlantic climate variability in CCSM3. *Journal of Climate*, *19*(11), 2451–2481. https://doi.org/10.1175/JCLI3759.1

Dong, L., & McPhaden, M. J. (2018). Unusually warm Indian Ocean sea surface temperatures help to arrest development of El Niño in 2014. *Scientific Reports*, *8*(1), 2249. https://doi.org/10.1038/s41598-018-20294-4

Fedorov, A. V. (2010). Ocean response to wind variations, warm water volume, and simple models of ENSO in the low-frequency approximation. *Journal of Climate*, *23*(14), 3855–3873. https://doi.org/10.1175/2010JCLI3044.1

Fedorov, A. V., Hu, S., Lengaigne, M., & Guilyardi, E. (2015). The impact of westerly wind bursts and ocean initial state on the development, and diversity of El Niño events. *Climate Dynamics*, *44*(5–6), 1381–1401. https://doi.org/10.1007/s00382-014-2126-4

Fedorov, A. V., Hu, S., Wittenberg, A. T., Levine, A. F. Z., & Deser, C. (2020). ENSO low-frequency modulation and mean state interactions (pp. 173–198). https://doi.org/10.1002/9781119548164.ch8

Fedorov, A. V., & Philander, S. G. (2000). Is El Niño changing? *Science*, *288*(5473), 1997–2002. https://doi.org/10.1126/science.288.5473.1997

Fedorov, A. V., & Philander, S. G. (2001). A stability analysis of tropical ocean–atmosphere interactions: Bridging measurements and theory for El Niño. *Journal of Climate*, *14*(14), 3086–3101. https://doi.org/10.1175/1520-0442(2001)014<3086:ASAOTO>2.0.CO;2

Ferrett, S., & Collins, M. (2019). ENSO feedbacks and their relationships with the mean state in a flux adjusted ensemble. *Climate Dynamics*, *52*(12), 7189–7208. https://doi.org/10.1007/s00382-016-3270-9

Ferster, B. S., Fedorov, A. V., Mignot, J., & Guilyardi, E. (2021). Sensitivity of the Atlantic meridional overturning circulation and climate to tropical Indian Ocean warming. *Climate Dynamics*, *5*, 1–19. https://doi.org/10.1007/s00382-021-05813-w

Ferster, B. S., Mignot, J., Fedorov, A., & Guilyardi, E. (2023a). Nudging the tropical Indian Ocean applied to the IPSL-CM6A-LR model - Control experiments (version v1) [Dataset]. Zenodo. https://doi.org/10.5281/zenodo.7579987

Ferster, B. S., Mignot, J., Fedorov, A., & Guilyardi, E. (2023b). Nudging the tropical Indian Ocean applied to the IPSL-CM6A-LR model - Cooling experiments (version v1) [Dataset]. Zenodo. https://doi.org/10.5281/zenodo.7590087

Ferster, B. S., Mignot, J., Fedorov, A., & Guilyardi, E. (2023c). Nudging the tropical Indian Ocean applied to the IPSL-CM6A-LR model - Warming experiments (version v1) [Dataset]. Zenodo. https://doi.org/10.5281/zenodo.7579970

Fletcher, C. G., & Cassou, C. (2015). The dynamical influence of separate teleconnections from the Pacific and Indian Oceans on the Northern Annular mode. *Journal of Climate*, *28*(20), 7985–8002. https://doi.org/10.1175/JCLI-D-14-00839.1

Fredriksen, H., Berner, J., Subramanian, A. C., & Capotondi, A. (2020). How does El Niño–Southern Oscillation change under global warming—A first look at CMIP6. *Geophysical Research Letters*, *47*(22), e2020GL090640. https://doi.org/10.1029/2020GL090640

Gill, A. E. (1980). Some simple solutions for heat-induced tropical circulation. *Quarterly Journal of the Royal Meteorological Society*, *106*(449), 447–462. https://doi.org/10.1002/qj.49710644905

Graham, F. S., Brown, J. N., Langlais, C., Marsland, S. J., Wittenberg, A. T., & Holbrook, N. J. (2014). Effectiveness of the Bjerknes stability index in representing ocean dynamics. *Climate Dynamics*, *43*(9–10), 2399–2414. https://doi.org/10.1007/s00382-014-2062-3

Guilyardi, E., Cai, W., Collin, M., Fedorov, A. V., Jin, F.-F., Kumar, A., et al. (2012). New strategies for evaluating ENSO processes in climate models. *Bulletin America Meteorology Social*, *93*(2), 235–238. https://doi.org/10.1175/bams-d-11-00106.1

Guilyardi, E., Wittenberg, A., Fedorov, A., Collins, M., Wang, C., Capotondi, A., et al. (2009). Understanding El Niño in Ocean–atmosphere general circulation models: Progress and challenges. *Bulletin of the American Meteorological Society*, *90*(3), 325–340. https://doi.org/10.1175/2008BAMS2387.1

Hardiman, S. C., Dunstone, N. J., Scaife, A. A., Smith, D. M., Knight, J. R., Davies, P., et al. (2020). Predictability of European winter 2019/20: Indian Ocean dipole impacts on the NAO. *Atmospheric Science Letters*, *21*(12), e1005. https://doi.org/10.1002/asl.1005

Heede, U. K., & Fedorov, A. V. (2021). Eastern equatorial Pacific warming delayed by aerosols and thermostat response to CO_2 increase. *Nature Climate Change*, *11*(8), 696–703. https://doi.org/10.1038/s41558-021-01101-x

Heede, U. K., & Fedorov, A. V. (2023a). Colder eastern equatorial Pacific and stronger walker circulation in the early 21st century: Separating the forced response to global warming from natural variability. *Geophysical Research Letters*, *50*(3), e2022GL101020. https://doi.org/10.1029/2022gl101020

Heede, U. K., & Fedorov, A. V. (2023b). Towards understanding the robust strengthening of ENSO and more frequent extreme El Niño events in CMIP6 global warming simulations. *Climate Dynamics*, *61*(5–6), 3047–3060. https://doi.org/10.1007/s00382-023-06856-x

Hu, S., & Fedorov, A. V. (2018). Cross-equatorial winds control El Niño diversity and change. *Nature Climate Change*, *8*(9), 798–802. https://doi.org/10.1038/s41558-018-0248-0

Hu, S., & Fedorov, A. V. (2019). Indian Ocean warming can strengthen the Atlantic meridional overturning circulation. *Nature Climate Change*, *9*(10), 747–751. https://doi.org/10.1038/s41558-019-0566-x

Jiang, W., Huang, P., Huang, G., & Ying, J. (2021). Origins of the excessive westward extension of ENSO SST simulated in CMIP5 and CMIP6 models. *Journal of Climate*, *34*(8), 2839–2851. https://doi.org/10.1175/JCLI-D-20-0551.1

Jin, F.-F. (1997). An equatorial Ocean recharge paradigm for ENSO. Part II: A stripped-down coupled model. *Journal of the Atmospheric Sciences*, *54*(7), 830–847. https://doi.org/10.1175/1520-0469(1997)054<0830:AEORPF>2.0.CO;2

Jin, F.-F., Chen, H., Zhao, S., Hayashi, M., Karamperidou, C., Stuecker, M. F., et al. (2020). Simple ENSO models (pp. 119–151). https://doi.org/10.1002/9781119548164.ch6

Jin, F.-F., Kim, S. T., & Bejarano, L. (2006). A coupled-stability index for ENSO. *Geophysical Research Letters*, *33*(23), L23708. https://doi.org/10.1029/2006GL027221

Lee, J., Planton, Y. Y., Gleckler, P. J., Sperber, K. R., Guilyardi, E., Wittenberg, A. T., et al. (2021). Robust evaluation of ENSO in climate models: How many ensemble members are needed? *Geophysical Research Letters*, *48*(20), e2021GL095041. https://doi.org/10.1029/2021GL095041

Liu, W., Duarte Cavalcante Pinto, D., Fedorov, A., & Zhu, J. (2023). The impacts of a weakened Atlantic meridional overturning circulation on ENSO in a warmer climate. *Geophysical Research Letters*, *50*(8), e2023GL103025. https://doi.org/10.1029/2023GL103025

Lu, B., Jin, F.-F., & Ren, H.-L. (2018). A coupled dynamic index for ENSO periodicity. *Journal of Climate*, *31*(6), 2361–2376. https://doi.org/10.1175/JCLI-D-17-0466.1

Lübbecke, J. F., & McPhaden, M. J. (2014). Assessing the 21st century shift in ENSO variability in terms of the Bjerknes stability index. *Journal of Climate*, *27*, 2577–2587. https://doi.org/10.1175/JCLI-D-13-00438.1

Luo, J. J., Sasaki, W., & Masumoto, Y. (2012). Indian Ocean warming modulates Pacific climate change. *Proceedings of the National Academy of Sciences of the United States of America*, *109*(46), 18701–18706. https://doi.org/10.1073/pnas.1210239109

Maher, N., Matei, D., Milinski, S., & Marotzke, J. (2018). ENSO change in climate projections: Forced response or internal variability? *Geophysical Research Letters*, *45*(20), 11390–11398. https://doi.org/10.1029/2018GL079764

Manucharyan, G. E., & Fedorov, A. V. (2014). Robust ENSO across a wide range of climates. *Journal of Climate*, *27*(15), 5836–5850. https://doi.org/10.1175/JCLI-D-13-00759.1

Matsuno, T. (1966). Quasi-geostrophic motions in the equatorial area. *Journal of the Meteorological Society of Japan. Ser. II*, *44*(1), 25–43. https://doi.org/10.2151/jmsj1965.44.1_25

Mayer, M., & Balmaseda, M. A. (2021). Indian Ocean impact on ENSO evolution 2014–2016 in a set of seasonal forecasting experiments. *Climate Dynamics*, *56*(7–8), 2631–2649. https://doi.org/10.1007/s00382-020-05607-6

McPhaden, M. J., Santoso, A., & Cai, W. (2020). Introduction to El Niño Southern Oscillation in a changing climate. In *Geophysical monograph series* (Vol. 253). https://doi.org/10.1002/9781119548164.ch1

Mignot, J., Hourdin, F., Deshayes, J., Boucher, O., Gastineau, G., Musat, I., et al. (2021). The tuning strategy of IPSL-CM6A-LR. *Journal of Advances in Modeling Earth Systems*, *13*(5), 1–34. https://doi.org/10.1029/2020ms002340

Milinski, S., Maher, N., & Olonscheck, D. (2020). How large does a large ensemble need to be? *Earth System Dynamics*, *11*(4), 885–901. https://doi.org/10.5194/esd-11-885-2020

Park, J., Lindberg, C. R., & Vernon, F. L. (1987). Multitaper spectral analysis of high-frequency seismograms. *Journal of Geophysical Research*, *92*(B12), 12675–12684. https://doi.org/10.1029/JB092iB12p12675

Planton, Y. Y., Guilyardi, E., Wittenberg, A. T., Lee, J., Gleckler, P. J., Bayr, T., et al. (2021). Evaluating climate models with the CLIVAR 2020 ENSO metrics package. *Bulletin of the American Meteorological Society*, *102*(2), E193–E217. https://doi.org/10.1175/BAMS-D-19-0337.1

Siuts, T., Bayr, T., & Lübbecke, J. F. (2022). Changes in ENSO characteristics in model simulations with considerably altered background climate states. *Journal of Climate*, *36*(2), 1–39. https://doi.org/10.1175/JCLI-D-21-1004.1

Stevenson, S., Wittenberg, A. T., Fasullo, J., Coats, S., & Otto-Bliesner, B. (2021). Understanding diverse model projections of future extreme El Niño. *Journal of Climate*, *34*(2), 449–464. https://doi.org/10.1175/JCLI-D-19-0969.1

Tan, X., Tang, Y., Lian, T., Zhang, S., Liu, T., & Chen, D. (2020). Effects of semistochastic westerly wind bursts on ENSO predictability. *Geophysical Research Letters*, *47*(14), e2019GL086828. https://doi.org/10.1029/2019GL086828

Thomson, D. J. (1982). Spectrum estimation and harmonic analysis. *Proceedings of the IEEE*, *70*(9), 1055–1096. https://doi.org/10.1109/PROC.1982.12433

Yeh, S.-W., Cai, W., Min, S.-K., McPhaden, M. J., Dommenget, D., Dewitte, B., et al. (2018). ENSO atmospheric teleconnections and their response to greenhouse gas forcing. *Reviews of Geophysics*, *56*(1), 185–206. https://doi.org/10.1002/2017RG000568

Yu, S., & Fedorov, A. V. (2022). The essential role of westerly wind bursts in ENSO dynamics and extreme events quantified in model "wind stress shaving" experiments. *Journal of Climate*, *35*(22), 1–62. https://doi.org/10.1175/jcli-d-21-0401.1

Zebiak, S. E., & Cane, M. A. (1987). A model El Niño–Southern Oscillation. *Monthly Weather Review*, *115*(10), 2262–2278. https://doi.org/10.1175/1520-0493(1987)115<2262:AMENO>2.0.CO;2

Zhang, L., & Karnauskas, K. B. (2017). The role of tropical interbasin SST gradients in forcing walker circulation trends. *Journal of Climate*, *30*(2), 499–508. https://doi.org/10.1175/JCLI-D-16-0349.1

Zhao, B., & Fedorov, A. (2020). The effects of background zonal and meridional winds on ENSO in a coupled GCM. *Journal of Climate*, *33*(6), 2075–2091. https://doi.org/10.1175/JCLI-D-18-0822.1